

Closed-Form Minkowski Sums of Convex Bodies with Smooth Positively Curved Boundaries

Sipu Ruan^a, Gregory S. Chirikjian^{a,b}

^a*Department of Mechanical Engineering, National University of Singapore, Singapore and the Laboratory for Computational Sensing and Robotics, Johns Hopkins University, Baltimore, USA*

^b*Address all correspondence to this author.*

Abstract

This paper proposes a closed-form parametric formula of the Minkowski sum boundary for broad classes of convex bodies in d -dimensional Euclidean space. With positive sectional curvatures at every point, the boundary that encloses each body can be characterized by the surface gradient. The first theorem directly parameterizes the Minkowski sums using the unit normal vector at each body surface. Although simple to express mathematically, such a parameterization is not always practical to obtain computationally. Therefore, the second theorem derives a more useful parametric closed-form expression using the gradient that is not normalized. In the special case of two ellipsoids, the proposed expressions are identical to those derived previously using geometric interpretations. In order to further examine the results, numerical verifications and comparisons of the Minkowski sums between two superquadric bodies are conducted. The application for the generation of configuration space obstacles in motion planning problems is introduced and demonstrated.

Keywords: Minkowski sums, computer-aided design, computational geometry

1. Introduction

Minkowski sums between two solid bodies have been studied for decades, and have wide applications in computer-aided design and manufacturing [1], computational geometry [2], robot motion planning [3], etc. This paper computes the boundary of a d -dimensional Minkowski sum, which is closely related to the $(d-1)$ -dimensional space when the two convex bodies touch each other without colliding. This space is also called the *contact space* in the context of robotics [4]. As a particular example in robot motion planning, the configuration space (C-space) of a robot is constructed by computing the Minkowski sums between

Email addresses: ruansp@jhu.edu (Sipu Ruan), mpegre@nus.edu.sg or gchirik1@jhu.edu (Gregory S. Chirikjian)

the robot parts at all possible orientations and the obstacles in the environment [5]. In this case, the robot is shrunk into a point and the boundaries of obstacles are inflated, resulting in *configuration-space obstacles (C-obstacles)*. Then a motion plan can be made for this point to traverse through the C-space. In addition, another class of applications includes the detection of contacts between two rigid bodies [6], as well as their separation distance or penetration depth [7]. The contact status between two bodies can be determined by querying the relative location between the Minkowski sums boundary and the point that the other body is shrunk into [8]. This method gives equivalent results with the one that directly and simultaneously finding a pair of points on the boundary surfaces with anti-parallel and opposite normal vectors [9]. Using an exact Minkowski sum expression is advantageous due to the reduced numbers of variables since only the point on the Minkowski sums boundary is searched.

In general, the computations of exact Minkowski sums can be very expensive [10]. A large amount of the investigations focus on bodies that are encapsulated by polytopes, with discrete and faceted surfaces [2, 11]. They are simple to be represented and stored in a modern computer, and can characterize a large range of convex or non-convex bodies through finite element methods. However, this type of surface is generally not smooth and requires a large set of parameters like vertices and faces information. In this paper, alternatively, we focus on a class of convex bodies whose boundary surfaces have implicit and parametric expressions. This class of surfaces is smooth and captures a wide variety of shapes with just a small number of parameters. And it is shown that for this wide class of convex bodies, it is possible to parameterize the boundary of their Minkowski sums in closed form. Note that the theoretical derivations throughout this paper are valid for any dimension, but for real application scenarios, we only discuss the 2D and 3D cases.

Previous work has shown that such a closed-form Minkowski sum boundary can be obtained between two ellipsoids [12], as well as when one of the two bodies is an ellipsoid and the other is enclosed by a general convex and differentiable surface [13, 8]. The methods used there were based on geometric interpretations by transforming the ellipsoid into a sphere and calculating an offset surface. This process limits at least one body to be an ellipsoid. In a broader class of bodies, this paper derives the closed-form boundary of Minkowski sums between two convex bodies with smooth boundaries having positive Gaussian curvature. The surfaces are parameterized by outward normal vectors [14, 9], which can be either normalized or un-normalized. Based on the two different parameterizations of the surfaces, two expressions for the closed-form Minkowski sums are derived, which are applicable to the bodies under general linear transformations such as rotation and shear. In the special case of ellipsoids, the proposed expressions of Minkowski sums boundary are identical with those from the previous geometric-based derivations.

The rest of this paper is organized as follows. Section 2 reviews related literature on the computational techniques for Minkowski sums. Section 3 reviews some useful properties of surfaces that are related to the derivations in this paper. Section 4 introduces the main results to compute the exact closed-form

Minkowski sums between two general bodies. Section 5 and 6 demonstrate the proposed expressions to the cases of ellipsoids and superquadrics. Section 7 numerically verifies the proposed method and compares the performance with the original definitions of Minkowski sums. Section 8 introduces an application of the proposed method in efficient generations of configuration-space obstacles in motion planning problems. Finally, section 9 concludes the paper.

2. Related Work

This section reviews related work on the computations of Minkowski sums. In general, if two bodies in \mathbb{R}^3 are non-convex, the complexity of computing their Minkowski sums can be as high as $O(m^3n^3)$, where m and n are the features (i.e. the number of facets) of the two polytopes. And the exact complexity bounds of Minkowski sums are rigorously analyzed in [10]. To make the calculations tractable, a large amount of efficient algorithms have been proposed, which can be generally grouped as decomposition-based, point-based and convolution-based methods.

The decomposition-based methods (either exact or approximated) segments the general polytopes into convex components [2, 15], since the complexity can be reduced to $O(mn)$ in the case of convex polytopes. The core idea behind is that the union of Minkowski sums is the Minkowski sums of the union of bodies. For this type of methods, the efficiency of convex decomposition affects the overall performance of the algorithms. In addition, point-based methods avoid using the expensive convex decomposition and computing the union of Minkowski sums [16, 17]. The major advantages are the ease of generating points than meshes, and the possibility of parallelisms [18]. But the local properties cannot be expressed by individual points themselves. Another type of methods is based on convolutions of two bodies, with the fact that Minkowski sum of two solid bodies is the support of the convolution of their indicator functions [19, 20, 11, 21]. Convolution-based methods were also widely applied into Minkowski sum computations between surfaces or curves with algebraic expressions [22, 23, 24, 25, 26]. Particularly, these methods constructs an offset surface or curve based on the shapes of the two bodies, and trims the portions that fall into the interior of the outer boundary.

For the case of bounding surfaces of two convex bodies, such a trimming can be omitted since their Minkowski sum is also convex. By applying this property, closed-form expressions of Minkowski sums have been proposed, with the cases when at least one body is ellipsoid [12, 13, 8]. These work calculated an offset surface in the affine space when one ellipsoid is transformed into a sphere. The expressions are exact and in closed-form. However, they require at least one body to be an ellipsoid, which limits the ability to extend for more complex shapes.

The goal of this paper is also to develop exact and closed-form expressions of Minkowski sums. But the two bodies are allowed to be within a more general class of convex bodies with positive Gaussian curvatures. The expressions are

parameterized in a totally different way as compared to the previous geometric-based method. The results are the same in the special case of ellipsoids.

3. Minkowski Sums and Geometric Properties of Surfaces

This section reviews several definitions and properties of Minkowski sums and surfaces that are necessary for the derivations throughout this paper.

3.1. Definition and computation of Minkowski sums

Given two solid bodies B_1 and B_2 in d -dimensional Euclidean space, their Minkowski sum is defined as

$$B_1 \oplus B_2 \doteq \{\mathbf{x} + \mathbf{y} \mid \mathbf{x} \in B_1, \mathbf{y} \in B_2\}. \quad (1)$$

In this paper, we specifically compute the boundary of Minkowski sums between B_1 and $-B_2$, i.e. $\partial[B_1 \oplus (-B_2)]$, where

$$B_1 \oplus (-B_2) \doteq \{\mathbf{x} - \mathbf{y} \mid \mathbf{x} \in B_1, \mathbf{y} \in B_2\}. \quad (2)$$

Geometrically, when placing B_2 at this boundary surface, B_1 and B_2 touch each other (without penetrating) outside. In the context of robotics, this boundary is also called the *contact space*, which divide the space of collision and separation. Note that $-B_2$ is the reflection of the original body B_2 with respect to its center. And if B_2 is central symmetric to itself (like an ellipsoid), Eqs. (1) and (2) are equivalent, i.e. $B_1 \oplus B_2 = B_1 \oplus (-B_2)$. Once this boundary is known, $B_1 \oplus (-B_2)$ can also be parameterized trivially.

If a set of points is sampled on the boundary of each surface, the Minkowski sums between these two bodies can be approximated as a discrete surface. Since both boundary surfaces are assumed to be convex, a direct way to compute the approximated Minkowski sums is to add all the points on different surfaces and take the convex hull of the result [27]. This refers to a direct method using the *definition* (Eq. (2)) of the Minkowski sums, which is applied to be compared with our closed-form method to be proposed.

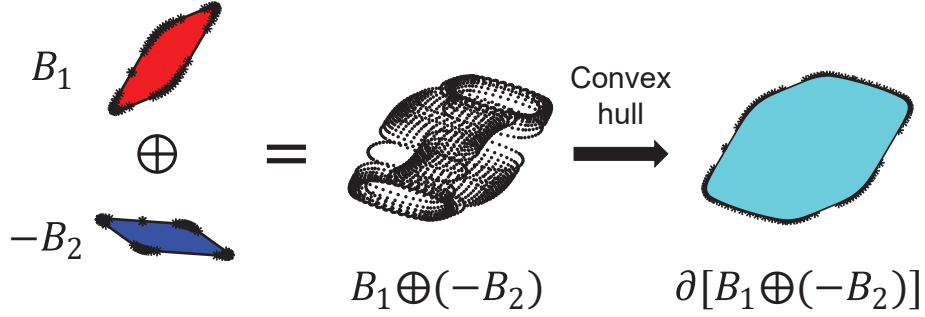
Figure 1 shows the process of computing Minkowski sums using the original definition as in Eq. (1) as well as our closed-form solution. The demonstrations in the 2D case are shown in the figure, and the boundaries of both bodies as well as their Minkowski sums are 1D curves. For both methods, the points on the bounding surfaces are sampled based on a set of angles $\theta_k \in [-\pi, \pi]$ that parameterize an 1D unit circle.

3.2. Some geometric properties of surfaces

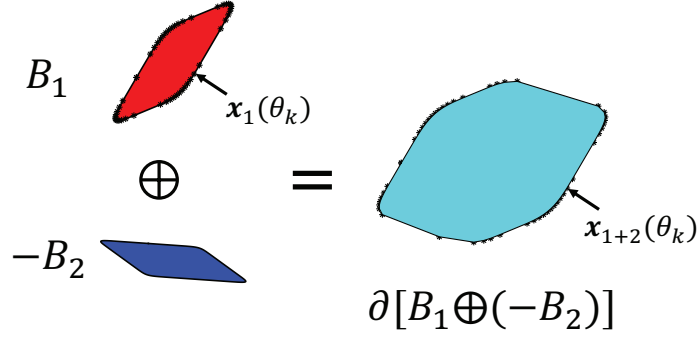
Suppose that the boundary of convex closed body B_i is defined by the parametric equation

$$\mathbf{x} = \mathbf{f}(\mathbf{u}) \in \mathbb{R}^d \quad (3)$$

where the unit vector $\mathbf{u} \in \mathbb{S}^{d-1}$ is in turn parameterized by $d - 1$ angles. A coordinate system can always be chosen such that the body B_i itself can be



(a) Computational process via the original Minkowski sums definition.



(b) Computational process of the closed-form solution.

Figure 1: Demonstration of the process to compute Minkowski sums using the original definition and our closed-form solutions. In (a), the surfaces enclosing both bodies are sampled into point sets; then all the pairs of points in different surfaces are added to obtain the Minkowski sums, i.e. $B_1 \oplus (-B_2)$; the boundary of Minkowski sums, i.e. $\partial[B_1 \oplus (-B_2)]$, is then computed via convex hull operation. In (b), only one of the body (i.e. B_1) surfaces is sampled, and the parameters (i.e. θ_k) of the points on Minkowski sums boundary is the same with those on the sampled body; in other words, $\mathbf{x}_{1+2}(\theta_k)$ is computed based on $\mathbf{x}_1(\theta_k)$ in closed-form. Here, $\theta_k \in [-\pi, \pi]$ is the sampled angle that parameterizes the boundary of a unit circle, i.e. $[\cos \theta_k, \sin \theta_k]^T$.

centered and parameterized as $\mathbf{x} = r\mathbf{f}(\mathbf{u})$ where $r \in [0, 1]$. Then the origin $\mathbf{0} \in B_i$. Here $\mathbf{f} : \mathbb{S}^{d-1} \rightarrow \mathbb{R}^d$ can be thought of as an embedding of the sphere which is deformed while ensuring the convexity of B_i . Consequently, the line segment connecting any two points in ∂B_i is fully contained in B_i .

Assume that the corresponding implicit equation of B_i exists and can be written as

$$\Psi(\mathbf{x}) = \Psi(\mathbf{f}(\mathbf{u})) = 1. \quad (4)$$

Thinking of $\mathbf{u} = \mathbf{u}(\phi_1, \dots, \phi_{d-1})$, the tangent vectors can be computed from Eq. (3) as

$$\mathbf{t}_i = \frac{\partial \mathbf{x}}{\partial \phi_i},$$

which, in general, is not orthonormal. Moreover, the outward pointing unit normal to the surface at the same point \mathbf{x} can be calculated as

$$\mathbf{n}(\mathbf{u}) \doteq \frac{(\nabla_x \Psi)(\mathbf{x})}{\|(\nabla_x \Psi)(\mathbf{x})\|} \Big|_{\mathbf{x}=\mathbf{f}(\mathbf{u})}. \quad (5)$$

The *Gauss map* assigns to each point $\mathbf{f}(\mathbf{u}) \in \partial B$ its normal $\mathbf{n}(\mathbf{u}) \in \mathbb{S}^{d-1}$. And the function $\mathbf{n} : \mathbb{S}^{d-1} \rightarrow \mathbb{S}^{d-1}$ is closely related. In this paper we will make extensive use of Eq. (5), as well as the un-normalized gradient

$$\mathbf{m}(\mathbf{u}) \doteq (\nabla_x \Psi)(\mathbf{x})|_{\mathbf{x}=\mathbf{f}(\mathbf{u})}. \quad (6)$$

The Gaussian curvature is the Jacobian determinant of the Gauss map. Consequently, if ∂B has positive Gaussian curvature everywhere, then the relationship $\mathbf{n} = \mathbf{n}(\mathbf{u})$ will be invertible as $\mathbf{u} = \mathbf{n}^{-1}(\mathbf{n}) \doteq \mathbf{u}(\mathbf{n})$. Then it becomes possible, at least in principle, to re-parameterize positions on the surface using the outward normal as

$$\mathbf{x} = \tilde{\mathbf{f}}(\mathbf{n}), \quad (7)$$

where $\tilde{\mathbf{f}}(\mathbf{n}) = \mathbf{f}(\mathbf{u}(\mathbf{n}))$. As with \mathbf{u} , it is possible to use angles to parameterize \mathbf{n} . When such a parameterization is used,

$$\frac{(\nabla_x \Psi)(\mathbf{x})}{\|(\nabla_x \Psi)(\mathbf{x})\|} \Big|_{\mathbf{x}=\tilde{\mathbf{f}}(\mathbf{n})} = \mathbf{n}. \quad (8)$$

4. Main Results

In this section, the main results of the paper are presented. We first propose two possible expressions for closed-form Minkowski sums, along with the proofs. Both of these theorems assume two bodies are in their canonical forms. Therefore, in the following result, we show the expression when linear transformations are applied to the two bodies. The expressions are demonstrated in the 2D case in Figs. 2 and 3.

4.1. Closed-form Minkowski sums parameterized by outward unit normal

Theorem 1: If the boundaries ∂B_1 and ∂B_2 of convex bodies B_1 and B_2 each have closed form parametric expressions of the form in Eq. (3) and their Gauss maps can be obtained in closed form resulting in parametric equations $\mathbf{x}_i = \tilde{\mathbf{f}}_i(\mathbf{n}_i)$, then their Minkowski sum boundary $\partial[B_1 \oplus (-B_2)]$ can be parameterized as

$$\boxed{\mathbf{x}_{1+2}(\mathbf{n}_1) = \tilde{\mathbf{f}}_1(\mathbf{n}_1) - \tilde{\mathbf{f}}_2(-\mathbf{n}_1)}, \quad (9)$$

where $\mathbf{n}_1 \in \mathbb{S}^{d-1}$ can be parameterized using spherical coordinates which in turn parameterize \mathbf{x}_{1+2} .

Proof: Hold B_1 fixed, and allow B_2 to move such that it kisses B_1 at any point on its surface. Record the surface that the origin of the reference frame attached to B_2 traces out as B_2 undergoes all translational motions for which $\partial B_1 \cap \partial B_2$ consists of a single point. When this occurs, the normals of both surfaces must pass through the point of contact, lie along a common line, and have opposite sense. The common point of contact between the two bodies will appear as $\tilde{\mathbf{f}}_1(\mathbf{n}_1)$ in the coordinate system of B_1 (i.e., the world frame), and as $\tilde{\mathbf{f}}_2(-\mathbf{n}_2)$ in the moving coordinate system attached to B_2 . The latter is described in the coordinate system in the world frame as the relative position vector $-\tilde{\mathbf{f}}_2(-\mathbf{n}_2)$. Adding both gives the result. \square

Figure 2 demonstrates the relationships of the outward normal vectors at each body boundary (i.e. \mathbf{n}_1) as well as different terms in the closed-form Minkowski sums expression as in Eq. (9). Though this can be done in principle, in practice it is often difficult to obtain in closed form expression for $\tilde{\mathbf{f}}_i(\mathbf{n}_i)$.

In such cases, it can be somewhat easier to parameterize \mathbf{x} in terms of its un-normalized gradient as

$$\mathbf{x} = \tilde{\mathbf{f}}(\mathbf{m}), \quad (10)$$

where \mathbf{m} is obtained from Eq. (6). Then it is possible to equate

$$\mathbf{f}(\mathbf{u}) = \tilde{\mathbf{f}}(\mathbf{n}) = \tilde{\mathbf{f}}(\mathbf{m})$$

because Eqs. (3), (7) and (10) are different parameterizations of the same boundary, i.e. ∂B . Once $\tilde{\mathbf{f}}(\mathbf{m})$ is obtained analytically, an explicit surface parameterization can be constructed by setting

$$\mathbf{m}(\phi) = \tilde{\mathbf{f}}^{-1}(\mathbf{f}(\mathbf{u}(\phi))). \quad (11)$$

In the case of Eq. (7), there is greater choice: Either the analogous computation can be done as

$$\mathbf{n}(\phi) = \tilde{\mathbf{f}}^{-1}(\mathbf{f}(\mathbf{u}(\phi))), \quad (12)$$

or we can simply choose to parameterize \mathbf{n} in the same way as $\mathbf{u}(\phi)$. That is, even though \mathbf{n} is not \mathbf{u} , in the final step \mathbf{u} is no longer part of the description and we can choose to parameterize the surface by letting $\mathbf{n} = \mathbf{u}(\phi)$. Hence these

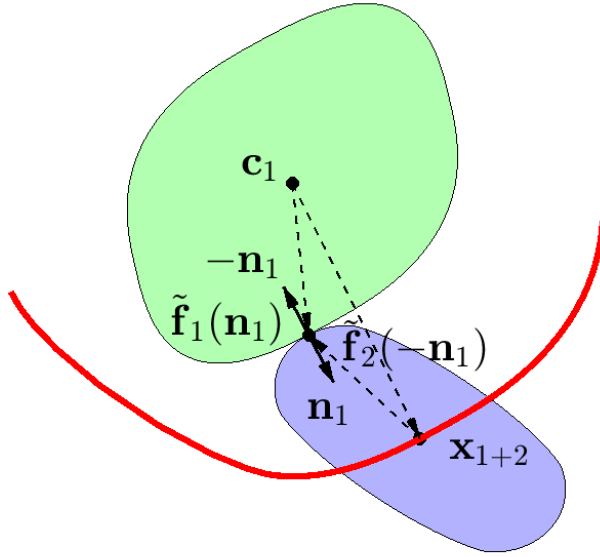


Figure 2: Demonstration of Theorem 1. The two bodies touch each other at only a point, which is parameterized by the unit outward normal vectors, i.e. $\tilde{\mathbf{f}}_1(\mathbf{n}_1)$ and $\tilde{\mathbf{f}}_2(-\mathbf{n}_1)$. The normal vectors at the contact point are anti-parallel to each other. The green and blue patched bodies are B_1 and B_2 respectively. \mathbf{c}_1 is the center of B_1 , and B_2 is placed at one of the Minkowski sums boundary point \mathbf{x}_{1+2} . The red curve is a section of the computed closed-form Minkowski sums boundary.

are two variants on this parameterization. The same choice does not exist for parameterizing $\mathbf{m}(\phi)$ because it is not a unit vector, and Eq. (11) is used. Note that by definition

$$(\nabla_x \Psi)(\mathbf{x})|_{\mathbf{x}=\tilde{\mathbf{f}}(\mathbf{m})} = \mathbf{m}. \quad (13)$$

And this leads to our second main result.

4.2. Closed-form Minkowski sums parameterized by un-normalized gradient

Theorem 2: If the boundaries ∂B_1 and ∂B_2 of convex bodies B_1 and B_2 each have closed form parametric expressions of the form in Eq. (10) and if it is possible to write $\|\mathbf{m}_2\| = \Phi(\mathbf{m}_1)$, where $\Phi(\cdot)$ has closed form, then the Minkowski sum boundary $\partial[B_1 \oplus (-B_2)]$ can be parameterized in closed form as

$$\mathbf{x}_{1+2}(\mathbf{m}_1) = \tilde{\mathbf{f}}_1(\mathbf{m}_1) - \tilde{\mathbf{f}}_2\left(-\frac{\Phi(\mathbf{m}_1)}{\|\mathbf{m}_1\|}\mathbf{m}_1\right), \quad (14)$$

where $\mathbf{m}_1 \in \mathbb{R}^d$ can be parameterized using the spherical coordinates of the original parametric expression for B_1 .

Proof: Using the same reasoning as in Theorem 1, for the bodies to kiss at a point their gradients must lie along the common normal line passing through the kissing point, and have opposite sense. Since $\mathbf{m}_i = \|\mathbf{m}_i\|\mathbf{n}_i$ ($i = 1, 2$), the appropriate match of gradients that will cause a point $\mathbf{x}_2(\mathbf{m}_2)$ in the frame attached to B_2 to kiss B_1 at the point $\mathbf{x}_1(\mathbf{m}_1)$ in the frame attached to B_1 , can be screened for by computing

$$\int_{\mathbb{S}^{d-1}} \delta(\mathbf{n}_1, \mathbf{n}_2) \tilde{\mathbf{f}}_2(-\|\mathbf{m}_2\|\mathbf{n}_2) d\mathbf{n}_2 = \tilde{\mathbf{f}}_2(-\|\mathbf{m}_2\|\mathbf{n}_1).$$

This can then be written as

$$\tilde{\mathbf{f}}_2\left(-\frac{\|\mathbf{m}_2\|}{\|\mathbf{m}_1\|}\mathbf{m}_1\right) = \tilde{\mathbf{f}}_2\left(-\frac{\Phi(\mathbf{m}_1)}{\|\mathbf{m}_1\|}\mathbf{m}_1\right).$$

Then, subtracting gives Eq. (14). \square

As a consequence of these theorems, it is easy to observe that when $B_2 = cB_1$,

$$\mathbf{x}_{1+2} = (1 + c)\mathbf{x}_1.$$

Figure 3 shows the relationships of each term in the expression derived in Eq. (14).

4.3. A sufficient condition for the computation of $\Phi(\mathbf{m}_1)$

In general, $\|\mathbf{m}_2\| = \Phi(\mathbf{m}_1)$ can be obtained when a sufficient condition is satisfied. The relationships between \mathbf{m}_1 and \mathbf{m}_2 in closed-form can be computed as follows.

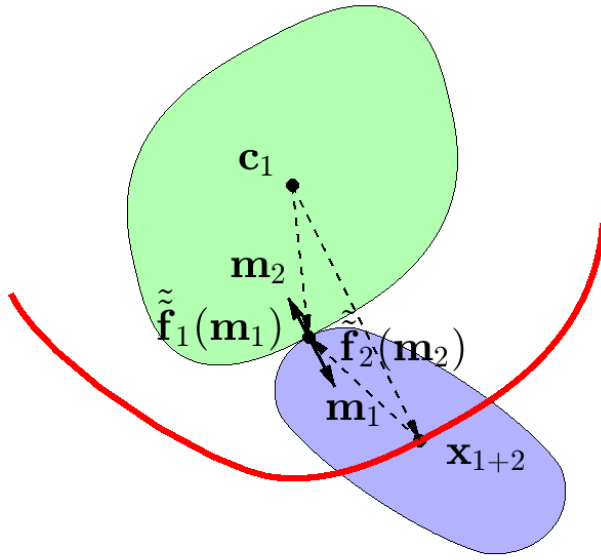


Figure 3: Demonstration of Theorem 2. The body boundaries are parameterized by the unnormalized gradients (\mathbf{m}_1 and \mathbf{m}_2), where $\mathbf{m}_2 = -\frac{\Phi(\mathbf{m}_1)}{\|\mathbf{m}_1\|} \mathbf{m}_1$. They are anti-parallel but have different magnitudes. The green and blue patched bodies are B_1 and B_2 respectively. \mathbf{c}_1 is the center of B_1 , and B_2 is placed at one of the Minkowski sums boundary point \mathbf{x}_{1+2} . The red curve is a section of the computed closed-form Minkowski sums boundary.

At the contact point, the outward normal vectors of the two surfaces are anti-parallel, with the relationship being

$$\frac{\mathbf{m}_2}{\|\mathbf{m}_2\|} = -\frac{\mathbf{m}_1}{\|\mathbf{m}_1\|}. \quad (15)$$

If \mathbf{m}_2 can be expressed in closed-form as a function of the unit vector \mathbf{u}_2 , i.e. $\mathbf{m}_2 = \mathbf{g}_2(\mathbf{u}_2)$, then Eq. (15) becomes

$$\frac{\mathbf{g}_2(\mathbf{u}_2)}{\|\mathbf{m}_2\|} = -\frac{\mathbf{m}_1}{\|\mathbf{m}_1\|}. \quad (16)$$

This means that $\mathbf{g}_2(\mathbf{u}_2)$ is proportional to $-\mathbf{m}_1$. If $\mathbf{g}_2(k\mathbf{u}_2) = \beta(k)\mathbf{g}_2(\mathbf{u}_2)$, then \mathbf{u}_2 is proportion to $\mathbf{g}_2^{-1}(-\mathbf{m}_1)$. Here, k is a constant scalar, and $\beta(k)$ is any scalar function of k , which is also a constant value. This condition is sufficient to derive the closed-form expression of $\|\mathbf{m}_2\| = \Phi(\mathbf{m}_1)$.

Since \mathbf{u}_2 is a unit vector, we get

$$\mathbf{u}_2 = \frac{\mathbf{g}_2^{-1}(\mathbf{m}_1)}{\|\mathbf{g}_2^{-1}(\mathbf{m}_1)\|}. \quad (17)$$

Then,

$$\|\mathbf{m}_2\| = \|\mathbf{g}_2(\mathbf{u}_2)\| = \left\| \mathbf{g}_2 \left(\frac{\mathbf{g}_2^{-1}(\mathbf{m}_1)}{\|\mathbf{g}_2^{-1}(\mathbf{m}_1)\|} \right) \right\| \doteq \Phi(\mathbf{m}_1). \quad (18)$$

4.4. General closed-form Minkowski sum expressions with linear transformations

Under invertible linear transformations from \mathbb{R}^d defined by $\mathbf{x}' = M\mathbf{x}$, tangents transform linearly as $\mathbf{t}_i \rightarrow M\mathbf{t}_i$. Alternatively, gradients transform as

$$(\nabla_{x'}\Psi)(M^{-1}\mathbf{x}')|_{\mathbf{x}'=M\mathbf{x}} = M^{-T}(\nabla_x\Psi)(\mathbf{x}). \quad (19)$$

This can be written as

$$\mathbf{m}' = M^{-T}\mathbf{m}, \quad (20)$$

where $M^{-T} \doteq (M^T)^{-1} = (M^{-1})^T$. This can be used together with $\tilde{\mathbf{f}}_i(\mathbf{m}_i)$ to get the Minkowski sum of linearly transformed parametric surfaces, by observing that the result of transforming by M is

$$\tilde{\mathbf{f}}'_i(\mathbf{m}'_i) = M_i\tilde{\mathbf{f}}_i(\mathbf{m}_i) = M_i\tilde{\mathbf{f}}_i(M_i^T\mathbf{m}'_i).$$

Then substituting either of these into Eq. (14) and expanding gives

$$\boxed{\mathbf{x}'_{1+2}(\mathbf{m}'_1) = M_1\tilde{\mathbf{f}}_1(M_1^T\mathbf{m}'_1) - M_2\tilde{\mathbf{f}}_2\left(-\frac{\Phi(M_2^T\mathbf{m}'_1)}{\|M_2^T\mathbf{m}'_1\|}M_2^T\mathbf{m}'_1\right)}, \quad (21)$$

and

$$\boxed{\mathbf{x}'_{1+2}(\mathbf{m}_1) = M_1\tilde{\mathbf{f}}_1(\mathbf{m}_1) - M_2\tilde{\mathbf{f}}_2\left(-\frac{\Phi(M_2^TM_1^{-T}\mathbf{m}_1)}{\|M_2^TM_1^{-T}\mathbf{m}_1\|}M_2^TM_1^{-T}\mathbf{m}_1\right)}. \quad (22)$$

5. Demonstration with Ellipsoids

This section demonstrates the proposed closed-form Minkowski sums between two ellipsoids. The results are compared with the ones coming from the previous geometric interpretations, which are the same. But using the derivations from this paper, the expressions are symmetrical and reflects the commutative property of Minkowski sums.

The surface of an ellipsoid can be parameterized as

$$\mathbf{f}(\mathbf{u}) = A\mathbf{u} \in \mathbb{R}^d \quad (23)$$

where $A = A^T \in \mathbb{R}^{d \times d}$ is a positive definite matrix, and $\mathbf{u} \in \mathbb{S}^{d-1}$, which can be parameterized by spherical angles $\phi = (\phi_1, \dots, \phi_{d-1})$. The corresponding implicit equation is

$$\Psi(\mathbf{x}) = 1 \text{ where } \Psi(\mathbf{x}) \doteq \mathbf{x}^T A^{-2} \mathbf{x}. \quad (24)$$

5.1. Demonstration of Theorem 1

Computing the normal as the normalized gradient, i.e.

$$\mathbf{n} = \frac{A^{-1}\mathbf{u}}{\|A^{-1}\mathbf{u}\|}.$$

This can be inverted to give

$$\mathbf{u} = \frac{A\mathbf{n}}{\|A\mathbf{n}\|}.$$

Then

$$\tilde{\mathbf{f}}(\mathbf{n}) = A \frac{A\mathbf{n}}{\|A\mathbf{n}\|}.$$

Then, from Theorem 1,

$$\mathbf{x}_{1+2}(\mathbf{n}_1) = \frac{A_1^2 \mathbf{n}_1}{\|A_1 \mathbf{n}_1\|} + \frac{A_2^2 \mathbf{n}_1}{\|A_2 \mathbf{n}_1\|}. \quad (25)$$

This is a variant of the formular given in [12] and the same as the formula derived in [28]. The unit vector $\mathbf{n}_1 \in \mathbb{S}^{d-1}$ can be parameterized with spherical angles $\phi = (\phi_1, \dots, \phi_{d-1})$ just like $\mathbf{u}(\phi)$, though it should not be confused with it.

5.2. Demonstration of Theorem 2

An alternative would be to parameterize ellipsoids according to Theorem 2. For two ellipsoids, i.e. $i = 1, 2$, we have

$$\mathbf{f}_i(\mathbf{u}_i) = A_i \mathbf{u}_i \quad (26)$$

and

$$(\nabla \Psi_i)(\mathbf{x}) = A_i^{-2} \mathbf{x}.$$

Substituting $\mathbf{x} = \tilde{\mathbf{f}}_i(\mathbf{m}_i)$ gives

$$A_i^{-2} \tilde{\mathbf{f}}_i(\mathbf{m}_i) = \mathbf{m}_i$$

or

$$\tilde{\mathbf{f}}_i(\mathbf{m}_i) = A_i^2 \mathbf{m}_i. \quad (27)$$

B_1 and B_2 will kiss at a point when

$$\frac{\mathbf{m}_1}{\|\mathbf{m}_1\|} = -\frac{\mathbf{m}_2}{\|\mathbf{m}_2\|}.$$

There is not enough information here to solve for \mathbf{m}_2 in terms of \mathbf{m}_1 . But from Eqs. (26) and (27),

$$\mathbf{m}_i = \tilde{\mathbf{f}}_i^{-1}(\mathbf{f}(\mathbf{u}_i)) = A_i^{-1} \mathbf{u}_i, \quad (28)$$

which means that the kissing condition can be written as

$$\frac{A_1^{-1} \mathbf{u}_1}{\|A_1^{-1} \mathbf{u}_1\|} = -\frac{A_2^{-1} \mathbf{u}_2}{\|A_2^{-1} \mathbf{u}_2\|}.$$

This equation says that \mathbf{u}_2 must be proportional to $-A_2 A_1^{-1} \mathbf{u}_1$, and the constraint that \mathbf{u}_2 is a unit vector then specifies that

$$\mathbf{u}_2 = -\frac{A_2 A_1^{-1} \mathbf{u}_1}{\|A_2 A_1^{-1} \mathbf{u}_1\|}.$$

Then using Eq. (28), we find that

$$\mathbf{m}_2 = \frac{-\mathbf{m}_1}{\|A_2 \mathbf{m}_1\|}$$

and so

$$\Phi(\mathbf{m}_1) \doteq \|\mathbf{m}_2\| = \frac{\|\mathbf{m}_1\|}{\|A_2 \mathbf{m}_1\|}.$$

Therefore,

$$\frac{\Phi(\mathbf{m}_1)}{\|\mathbf{m}_1\|} = \frac{1}{\|A_2 \mathbf{m}_1\|}.$$

Then Theorem 2 states that

$$\mathbf{x}_{1+2} = A_1^2 \mathbf{m}_1 + A_2^2 \frac{\mathbf{m}_1}{\|A_2 \mathbf{m}_1\|}. \quad (29)$$

Then substituting $\mathbf{m}_1 = A_1^{-1} \mathbf{u}_1$ with \mathbf{u}_1 parameterized as $\mathbf{u}_1(\phi)$ gives

$$\mathbf{x}_{1+2}(\phi) = A_1 \mathbf{u}(\phi) + \frac{A_2^2 A_1^{-1} \mathbf{u}(\phi)}{\|A_2 A_1^{-1} \mathbf{u}(\phi)\|}. \quad (30)$$

This is the same as the closed-form formula derived in a completely different way in [12].

5.3. Demonstration of transformations

Ellipsoids can be viewed as linearly transformed versions of spheres. For a sphere,

$$\mathbf{f}(\mathbf{u}) = \mathbf{u}$$

and since

$$\mathbf{n} = \mathbf{m} = \mathbf{u}$$

we have

$$\tilde{\mathbf{f}}(\mathbf{n}) = \mathbf{n} \text{ and } \tilde{\mathbf{f}}(\mathbf{m}) = \mathbf{m}.$$

Viewing the Minkowski sum of two ellipsoids as that of two transformed spheres, where $M_i = A_i$, then $\mathbf{m}'_i = A_i^{-1}\mathbf{u}$ and $\mathbf{m}_i = \mathbf{u}$ and Eqs. (21) and (22) both reduce to (29).

6. Demonstration with Superquadrics

We now examine more general types of bodies, with superquadrics being typical examples. The Minkowski sums can also be parameterized by their unnormalized gradients. The two theorems as well as the transformed version in both 2D and 3D cases are demonstrated with derivations of the intermediate expressions necessary to use the general formulas in Eq. (21) and (22).

6.1. Planar case

A planar superquadric can be parameterized as

$$\mathbf{x}(\mathbf{u}(\theta)) = \begin{pmatrix} a \cos^\epsilon \theta \\ b \sin^\epsilon \theta \end{pmatrix} \quad (31)$$

where $\epsilon \in (0, 2)$ to ensure the convexity of the body. With

$$\mathbf{u}(\theta) = \begin{pmatrix} \cos \theta \\ \sin \theta \end{pmatrix},$$

this means that

$$\mathbf{f}(\mathbf{u}) = \begin{pmatrix} a u_1^\epsilon \\ b u_2^\epsilon \end{pmatrix},$$

where the un-bolded u_i is the i -th entry of the vector \mathbf{u} . The corresponding normal vector is

$$\mathbf{m}(\theta) = \frac{2}{\epsilon} \begin{pmatrix} a^{-1} \cos^{2-\epsilon} \theta \\ b^{-1} \sin^{2-\epsilon} \theta \end{pmatrix},$$

and the square of its magnitude is

$$\|\mathbf{m}(\theta)\|^2 = a^{-2} \cos^{4-2\epsilon} \theta + b^{-2} \sin^{4-2\epsilon} \theta.$$

The implicit equation for this planar superquadric (or superellipse) is

$$\Psi(\mathbf{x}) = \left(\frac{x_1}{a}\right)^{2/\epsilon} + \left(\frac{x_2}{b}\right)^{2/\epsilon} = 1. \quad (32)$$

The gradient is then

$$(\nabla\Psi)(\mathbf{x}) = \begin{pmatrix} \frac{2}{\epsilon a} \left(\frac{x_1}{a}\right)^{2/\epsilon-1} \\ \frac{2}{\epsilon b} \left(\frac{x_2}{b}\right)^{2/\epsilon-1} \end{pmatrix} \doteq \mathbf{m} = \begin{pmatrix} m_1 \\ m_2 \end{pmatrix}.$$

Raising each component of this to the power $\epsilon/(2-\epsilon)$, and solving for \mathbf{x} , it is easy to reparameterize Eq. (31) in terms of \mathbf{m} as

$$\tilde{\mathbf{f}}(\mathbf{m}) = \begin{pmatrix} a \left(\frac{2}{\epsilon a}\right)^{\frac{-\epsilon}{2-\epsilon}} m_1^{\frac{\epsilon}{2-\epsilon}} \\ b \left(\frac{2}{\epsilon b}\right)^{\frac{-\epsilon}{2-\epsilon}} m_2^{\frac{\epsilon}{2-\epsilon}} \end{pmatrix}.$$

Theorem 2 is used here to compute the closed-form expression of Minkowski sums by first obtaining the relationships between \mathbf{m}_2 and \mathbf{u}_2 as

$$\mathbf{m}_2 = \mathbf{g}_2(\mathbf{u}_2) = \begin{pmatrix} \frac{2}{a_2\epsilon_2} u_{21}^{2-\epsilon_2} \\ \frac{2}{b_2\epsilon_2} u_{22}^{2-\epsilon_2} \end{pmatrix}, \quad (33)$$

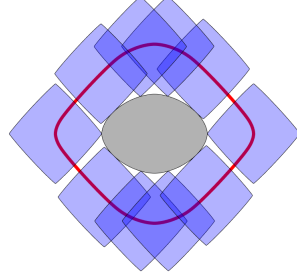
where $u_{2j} = \mathbf{u}_2 \cdot \mathbf{e}_j$ and \mathbf{e}_j is the j -th unit Cartesian coordinate basis, and the un-bolded a_2, b_2 and ϵ_2 denote the shape parameters of B_2 . Observing that $\mathbf{g}_2(k\mathbf{u}_2) = k^{2-\epsilon_2} \mathbf{g}_2(\mathbf{u}_2)$, the sufficient condition for this mapping is satisfied. So we are able to express $\|\mathbf{m}_2\|$ as a function of \mathbf{m}_1 using Eq. (18). The reverse function of \mathbf{g}_2 as a function of \mathbf{m}_1 is then explicitly computed as

$$\mathbf{g}_2^{-1}(\mathbf{m}_1) = \begin{pmatrix} \left(\frac{a_2\epsilon_2}{2} m_{11}\right)^{1/(2-\epsilon_2)} \\ \left(\frac{b_2\epsilon_2}{2} m_{12}\right)^{1/(2-\epsilon_2)} \end{pmatrix}, \quad (34)$$

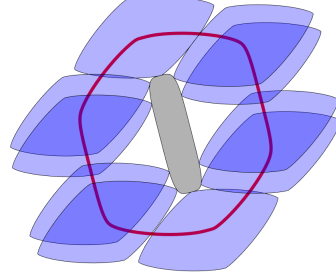
where $m_{1j} = \mathbf{m}_1 \cdot \mathbf{e}_j$ denotes the j -th entry of the gradient vector of B_1 . Finally, substituting Eqs. (33) and (34) into Eq. (18) gives the closed-form expression of $\|\mathbf{m}_2\|$.

Furthermore, using Eq. (22), we demonstrate the closed-form Minkowski sums under different linear transformations for the two superellipses, including:

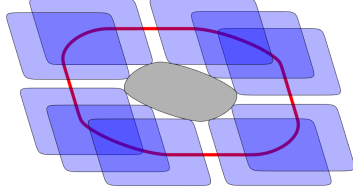
- pure rotations, i.e. $M_i^{(1)} = \text{rot}(\alpha_i) = \begin{pmatrix} \cos \alpha_i & -\sin \alpha_i \\ \sin \alpha_i & \cos \alpha_i \end{pmatrix}$, where α is the rotational angle ;
- pure shear, i.e. $M_i^{(2)} = \text{shear}(s_i) = \begin{pmatrix} 1 & s_i \\ 0 & 1 \end{pmatrix}$, where s is the magnitude of the shear transformation ;
- a combination of them, i.e. $M_i^{(3)} = \text{rot}(\alpha_i) \text{shear}(s_i)$.



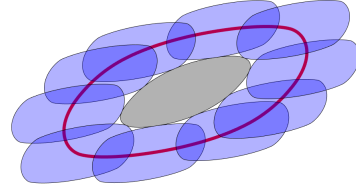
(a) Canonical forms.



(b) Pure rotations.



(c) Pure shear transformations.



(d) Combining rotation and shear.

Figure 4: Demonstration of the closed-form Minkowski sums for two 2D superquadrics in canonical forms and under linear transformations. B_1 is plotted in grey color at the center. The red curve represents the computed closed-form Minkowski sums boundary. B_2 is plotted in blue color and placed at 10 different locations on the Minkowski sums boundary.

Note that the right parenthesized superscript denotes the different types of transformation, and the right subscript denotes the i -th body.

Figure 4 demonstrates the expressions using different types of convex superellipses with $\epsilon \in (0, 2)$. B_1 is drawn in the center as a black curve, B_2 is drawn in blue and translates along the closed-form Minkowski sums boundary (in red) so as to kiss B_1 . The demonstrations include superellipses in their canonical forms and under different types of linear transformations such as rotations and shear transformations.

6.2. Spatial case

The implicit expression for a 3D superquadric surface is

$$\Psi(\mathbf{x}) = \left(\left(\frac{x_1}{a} \right)^{2/\epsilon_2} + \left(\frac{x_2}{b} \right)^{2/\epsilon_2} \right)^{\epsilon_2/\epsilon_1} + \left(\frac{x_3}{c} \right)^{2/\epsilon_1} = 1, \quad (35)$$

and the gradient is

$$(\nabla\Psi)(\mathbf{x}) = \begin{pmatrix} \frac{2}{a\epsilon_1} [\psi(x_1, x_2)]^{\epsilon_2/\epsilon_1-1} \left(\frac{x_1}{a}\right)^{2/\epsilon_2-1} \\ \frac{2}{b\epsilon_1} [\psi(x_1, x_2)]^{\epsilon_2/\epsilon_1-1} \left(\frac{x_2}{b}\right)^{2/\epsilon_2-1} \\ \frac{2}{c\epsilon_1} \left(\frac{x_3}{c}\right)^{2/\epsilon_1-1} \end{pmatrix} \doteq \mathbf{m} = \begin{pmatrix} m_1 \\ m_2 \\ m_3 \end{pmatrix}, \quad (36)$$

where $\psi(x_1, x_2) = \left(\frac{x_1}{a}\right)^{2/\epsilon_2} + \left(\frac{x_2}{b}\right)^{2/\epsilon_2}$ denotes the part in the implicit expression that includes coordinates x_1 and x_2 , and $\epsilon_1, \epsilon_2 \in (0, 2)$ to ensure the convexity of the body enclosed by the bounding surface.

Directly solving Eq. (36) for x_1, x_2, x_3 gives

$$\tilde{\mathbf{f}}(\mathbf{m}) = \begin{pmatrix} a \left(\frac{a\epsilon_1}{2} m_1\right)^{\epsilon_2/(2-\epsilon_2)} [\gamma(m_3)]^{(\epsilon_1-\epsilon_2)/(2-\epsilon_2)} \\ b \left(\frac{b\epsilon_1}{2} m_2\right)^{\epsilon_2/(2-\epsilon_2)} [\gamma(m_3)]^{(\epsilon_1-\epsilon_2)/(2-\epsilon_2)} \\ c \left(\frac{c\epsilon_1}{2} m_3\right)^{\epsilon_1/(2-\epsilon_1)} \end{pmatrix},$$

where

$$\gamma(m_3) = 1 - \left(\frac{c\epsilon_1}{2} m_3\right)^{2/(2-\epsilon_1)}.$$

On the other hand, Eq. (36) can be written with respect to the unit vector

$$\mathbf{u}(\eta, \omega) = \begin{pmatrix} \cos \eta \cos \omega \\ \cos \eta \sin \omega \\ \sin \eta \end{pmatrix} \doteq \begin{pmatrix} u_1 \\ u_2 \\ u_3 \end{pmatrix}$$

as

$$(\nabla\Psi)(\eta, \omega) = \begin{pmatrix} \frac{2}{a\epsilon_1} \cos^{2-\epsilon_1} \eta \cos^{2-\epsilon_2} \omega \\ \frac{2}{b\epsilon_1} \cos^{2-\epsilon_1} \eta \sin^{2-\epsilon_2} \omega \\ \frac{2}{c\epsilon_1} \sin^{2-\epsilon_1} \eta \end{pmatrix}.$$

Substituting η, ω in terms of u_1, u_2, u_3 , we get the explicit expressions that are necessary to compute $\Phi(\mathbf{m}_1)$ as

$$\mathbf{m}_2 = \mathbf{g}_2(\mathbf{u}_2) = \begin{pmatrix} \frac{2}{a_2\epsilon_{21}} u_{21}^{2-\epsilon_{22}} (u_{21}^2 + u_{22}^2)^{(\epsilon_{22}-\epsilon_{21})/2} \\ \frac{2}{b_2\epsilon_{21}} u_{22}^{2-\epsilon_{22}} (u_{21}^2 + u_{22}^2)^{(\epsilon_{22}-\epsilon_{21})/2} \\ \frac{2}{c_2\epsilon_{21}} u_{23}^{2-\epsilon_{21}} \end{pmatrix}, \quad (37)$$

where $a_2, b_2, c_2, \epsilon_{21}$ and ϵ_{22} are the shape parameters of B_2 , and $u_{2j} = \mathbf{u}_2 \cdot \mathbf{e}_j$ is the j -th entry of the vector \mathbf{u}_2 of B_2 . It can also be observed that, $\mathbf{g}_2(k \mathbf{u}_2) = k^{2-\epsilon_{21}} \mathbf{g}_2(\mathbf{u}_2)$, which satisfies the sufficient condition. Then the reverse function $\mathbf{g}_2^{-1}(\mathbf{m}_1)$ can be computed as

$$\mathbf{g}_2^{-1}(\mathbf{m}_1) = \begin{pmatrix} \left(\frac{a_2\epsilon_{21}}{2} m_{11}\right)^{\frac{1}{2-\epsilon_{22}}} [\rho(m_{21}, m_{22})]^{\frac{\epsilon_{21}-\epsilon_{22}}{4-2\epsilon_{21}}} \\ \left(\frac{b_2\epsilon_{21}}{2} m_{12}\right)^{\frac{1}{2-\epsilon_{22}}} [\rho(m_{21}, m_{22})]^{\frac{\epsilon_{21}-\epsilon_{22}}{4-2\epsilon_{21}}} \\ \left(\frac{c_2\epsilon_{21}}{2} m_{13}\right)^{\frac{1}{2-\epsilon_{21}}} \end{pmatrix}, \quad (38)$$

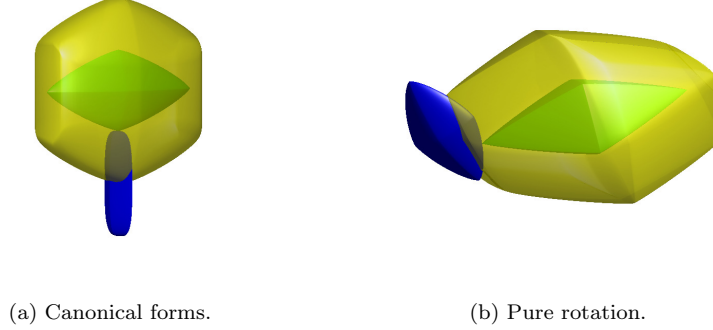


Figure 5: Demonstration of the closed-form Minkowski sums for two 3D superquadrics in canonical forms and with different orientations. B_1 is shown in green color at the center. The yellow surface represents the computed closed-form Minkowski sums boundary. B_2 is plotted in blue color and placed at one location on the Minkowski sums boundary.

where

$$\rho(m_{21}, m_{22}) = \left(\frac{a_2 \epsilon_{21}}{2} m_{21} \right)^{\frac{2}{2-\epsilon_{22}}} + \left(\frac{b_2 \epsilon_{21}}{2} m_{22} \right)^{\frac{2}{2-\epsilon_{22}}},$$

and $m_{ij} = \mathbf{m}_i \cdot \mathbf{e}_j$ is the j -th entry of the gradient vector \mathbf{m}_i of B_i .

The closed-form Minkowski sums for B_1 and B_2 in different orientations are visualized here, as shown in Fig. 5. B_1 is drawn in the center in green, and B_2 is drawn in blue and translates along the closed-form Minkowski sums boundary, which only kisses B_1 at every point.

7. Numerical Validations and Benchmarks in Simulation for the Closed-form Minkowski Sums

To validate the correctness and evaluate the performance of the proposed closed-form Minkowski sums, we conduct numerical simulations and compare with the discrete Minkowski sums computations from definition as shown in Fig. 1a.

At first, a set of points on the Minkowski sums boundary is generated using the proposed exact closed-form expression. And we examine, when placing B_2 at these points, whether there exists a kissing point that locates on both body boundary surfaces and the corresponding normal vectors are anti-parallel. To evaluate the efficiency of the proposed closed-form expression, we conduct benchmarks in the second simulation. The numbers of points on the boundaries of S_1 and S_2 are varied, and the running time to generate the point set on the Minkowski sums boundary are compared. All the simulations throughout this paper are implemented in Matlab R2018b and performed in an Intel Core i7 CPU at 2.70 GHz.

7.1. Numerical validations for the closed-form Minkowski sums computations

The general idea is to compute the kissing point of the two bodies when placing B_2 at each point on Minkowski sum boundary. We are using the fact that the kissing point \mathbf{x}_{kiss} between two bodies must satisfies:

- The kissing point lies on both surfaces. This can be achieved when the implicit expression at the kissing point equals to one, i.e.

$$\Psi_1({}^1\mathbf{x}_{kiss}) = \Psi_2({}^2\mathbf{x}_{kiss}) = 1, \quad (39)$$

where $\Psi_i(\cdot)$ is the implicit expression of the i -th body and ${}^i\mathbf{x}_{kiss}$ is the kissing point as viewed in the body frame of i -th body.

- The normal vectors at the kissing point with respect to the two surfaces are anti-parallel. Specifically, we can compute the un-normalized gradients at the kissing point on each surface, and verify that the angle between them is π .

In practice, we first sample a set of points $\mathbf{x}_1(\phi_k)$ on ∂B_1 based on the set of angular parameters $\{\phi_k\}$. Then, this parameter set can also be used to generate the points on Minkowski sum $\mathbf{x}_{1+2}(\phi_k)$ using our closed-form expression. Then, we place B_2 at $\mathbf{x}_{1+2}(\phi_k)$, and verify that each $\mathbf{x}_1(\phi_k)$ is the kissing point.

To validate the first condition that the kissing point locates on both bounding surfaces, $\mathbf{x}_1(\phi_k)$ is transformed into the local frame of each body, then Eq. (39) can be examined. Note that, since \mathbf{x}_1 is computed from the parametric expression of B_1 , we only need to verify that the value of

$$e_{implicit} \doteq |\Psi_2({}^2\mathbf{x}_1) - 1| = 0. \quad (40)$$

Then, since the gradient can be computed from the point on surface, the un-normalized gradients at the candidate kissing point on both bodies can be computed as $\mathbf{m}_1(\mathbf{x}_1)$ and $\mathbf{m}_2(\mathbf{x}_1)$ respectively. They are anti-parallel when

$$e_{gradient} \doteq \left| \frac{\mathbf{m}_1(\mathbf{x}_1) \cdot \mathbf{m}_2(\mathbf{x}_1)}{\|\mathbf{m}_1(\mathbf{x}_1)\| \|\mathbf{m}_2(\mathbf{x}_1)\|} - \cos(\pi) \right| = 0. \quad (41)$$

Once these two conditions are verified, we can say that \mathbf{x}_1 is the kissing point when B_2 is place at the Minkowski sum boundary.

We conduct simulations to verify in both 2D and 3D cases. For 2D case, a total of 1000 points are sampled on ∂B_1 based on the angular parameter set $\{\phi_k^{2D}\} = \{\theta_k\}$; and for 3D case, 100 samples are generated for each angular parameter pair (i.e. $\{\phi_k^{3D}\} = \{(\eta_k, \omega_k)\}$), so a total of 10^4 points are sampled on ∂B_1 . And for both cases, 100 trials are simulated and the mean values of Eq. (40) and (41) for among all the trials are computed.

For the 2D case, among all the trials, the mean values of $e_{implicit}$ and $e_{gradient}$ are 5.9194×10^{-16} and 6.1839×10^{-7} , respectively. And for the 3D case, the mean values of $e_{implicit}$ and $e_{gradient}$ are 1.8303×10^{-9} and 4.0654×10^{-7} , respectively. The results show that when B_2 is centered at the Minkowski sum boundary

points $\mathbf{x}_{1+2}(\phi)$, which are computed by both our proposed closed-form expression, there exists a kissing point $\mathbf{x}_1(\phi)$. Ideally, the expressions in Eq. (40) and (41) should equal to zero since our proposed closed-form Minkowski sums expression is the exact solution. Due to the numerical precision issues, there are discrepancies between the computational results and the ideal expectations. However, these discrepancies are all very small, i.e. less than the level of 10^{-6} , which is acceptable for the numerical verification purposes. Therefore, the point on ∂B_1 parameterized by ϕ_k is the kissing point when placing B_2 at $\mathbf{x}_{1+2}(\phi_k)$, with which the proposed closed-form Minkowski sum expression is numerical verified.

7.2. Benchmarks for computational time of the point sets on Minkowski sums boundary

To evaluate the performance of computing a discrete point set on the Minkowski sums boundary, the running time is measured for our proposed method and the method using the original definition. Note that for the Minkowski sums computed from definition, we represent the discrete boundaries of both surfaces as point sets. Since the two bodies are convex, the corresponding Minkowski sums boundary is the convex hull of the summations of all possible pairs from the two point sets. Although it is not an exact result, we could still get a sense of the quality of our closed-form computation compared to the definition of Minkowski sums.

To give an impression of the computational speed of our proposed method, the running time for both 2D and 3D cases are compared. In principle, the running time for ours only depend on the number of points sampled on ∂B_1 , while the brute-force method depends on the sampled points on both body surfaces. Therefore, we expect that ours can achieve a linear time complexity with respect to the number of sampled vertices, while the brute-force method would be much slower. Figure 6 compares the running time for the two methods of computing Minkowski sums at different discretization levels over the 100 experiment trials.

From the comparison results, our proposed closed-form expressions for Minkowski sums achieve a linear time complexity with respect to the number of vertices on one body surface. This outperforms the method that computes the discrete Minkowski sums by definition, which is increases much faster when more vertices are sampled. Furthermore, since we find a relationship based on the outward normal at the touching point, the number of the points on Minkowski sum boundary only depends on one body where the normal is computed. This explains the linear complexity with respect to the number of vertices on one body surface. Through this nice property, the Minkowski sums boundary can be computed in a very efficient way, which provides quite an advantage especially in the 3D case.

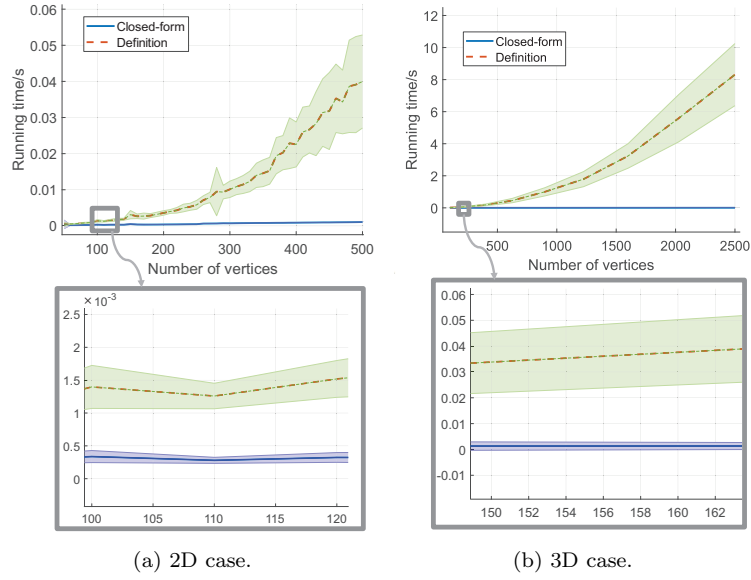


Figure 6: Running time comparisons for the closed-form and brute-force calculations of Minkowski sums. For both sub-figures, curves represent the mean value of the running time, and the shaded regions show the range of the standard deviation. The blue curve denotes our proposed method, while the orange curve denotes the method using definition. A zoom-in view of a small region when the number of vertices is small is shown below each sub-figure.

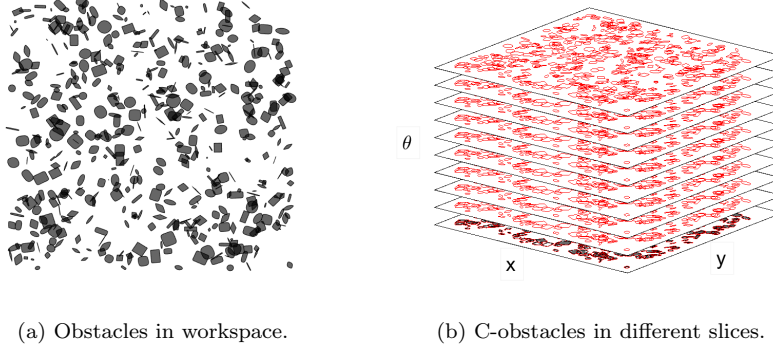


Figure 7: Demonstration of the C-obstacles generation in SE(2). The figures show the trial when 500 obstacles are located arbitrarily in the environment and the corresponding C-obstacles for 10 sampled orientations of the robot. Obstacles in the workspace are represented by black superellipses, and the calculated Minkowski sums in each C-slice are represented in red.

8. Application on Point-based Configuration Space Obstacles Generations

One of the important applications of Minkowski sums is to generate configuration space obstacles [3] in robot motion planning algorithms. The idea is to shrink the robot into a single point and inflate all obstacles by the Minkowski sums boundaries. Then a motion planner can be developed for the point robot that avoids the inflated obstacles, which are called *configuration-space obstacles* (*C-obstacles*). If the robot is bounded by a circle or sphere, then, the current space is the configuration space of the robot. But if the robot is enclosed by other kinds of geometric shapes, i.e. the superquadrics, then the orientation matters. In this case, multiple *slices* [29] of the configuration space are required to be generated, each of which requires the computations of the C-obstacles using Minkowski sums. Such a class of planners are effective when the robot is rigid, i.e. mobile robot, drone, underwater vehicle, etc, where the Minkowski sums computation take a very essential role.

Here we show that using our proposed closed-form Minkowski sums, C-obstacles for rigid-body robots in multiple orientations can be calculated efficiently in both 2D and 3D cases. Both the robot and obstacles are generated as superquadric bodies with arbitrary shape parameters. We measure the computational time for generating the C-obstacle boundary points for a set of orientations of the robot and multiple numbers of obstacles. The Minkowski sums for all obstacles are computed in pairwise with the robot in a loop. Figure 7 demonstrates the simulation for C-obstacles generation in SE(2) configuration space. This demonstration includes 500 obstacles in the environment with arbitrary shapes and poses. And 10 slices of the configuration space with the computed C-obstacles are shown.

Table 1: Parameters and running time for C-obstacle generations in both 2D and 3D workspaces.

Dim.	Num. obstacles	Num. points	Num. orientations	Total time (s)	Avg. time per point (μs)
2D	50	50	50	0.41	3.280
2D	1000	50	50	7.07	2.828
2D	10000	50	50	71.36	2.854
3D	50	100	30	1.07	7.133
3D	1000	100	30	20.63	6.877
3D	10000	100	30	199.13	6.638

Table 1 summarizes the parameters and the running time results of generating C-obstacles in both 2D and 3D cases. The parameters include the numbers of obstacles, computed Minkowski sum boundary points and the orientations of the robot. And for the running time, the total computational time for all the points generated on all obstacles and the averaged time for each point on the Minkowski sum boundary are measured.

The simulation shows a potential application of our closed-form Minkowski sums computations in generating C-obstacles, which is essential in developing efficient motion planning algorithms for rigid-body robots. The performance are based on a Matlab implementation without GPU or parallel computing accelerations, which achieves a level of seconds for hundreds of obstacles and minutes for thousands of obstacles. On average, the closed-form computation for each boundary point is in the level of microseconds. With these points on the boundary of C-obstacles, the collision-free configuration space can then be characterized, which leads to various efficient motion planners [29, 13].

9. Conclusion

This paper introduces a novel exact and closed-form parameterization of Minkowski sums between two positively curved bodies in d -dimensional Euclidean space. The boundary surface of each body is parameterized as a function of the gradient. It is shown that the Minkowski sums can be derived in closed-form based on the surface gradient that can be either normalized (i.e. becomes the outward normal vector) or un-normalized. The results proposed in this paper, both in canonical form and with linear transformations, are identical with those using geometrical interpretation in the case of two ellipsoids. And in general, these expressions can be applied to pairs of bodies that are enclosed by general smooth surfaces with positive Gaussian curvature at every point. Numerical simulations are conducted in the case of two superquadrics, showing the correctness and efficiency of the proposed closed-form expression. An application in generating configuration-space obstacles for motion planning algorithms is introduced and demonstrated.

Acknowledgement

This work was performed under U.S National Science Foundation grants IIS-1619050 and CCF-1640970 and U.S. Office of Naval Research Award N00014-17-1-2142. The ideas expressed in this paper are solely those of the authors.

References

- [1] R. C. Evans, M. A. O'Connor, J. R. Rossignac, Construction of Minkowski sums and derivatives morphological combinations of arbitrary polyhedra in CAD/CAM systems, US Patent 5,159,512 (Oct. 27 1992).
- [2] G. Varadhan, D. Manocha, Accurate Minkowski sum approximation of polyhedral models, in: 12th Pacific Conference on Computer Graphics and Applications, 2004. PG 2004. Proceedings., IEEE, 2004, pp. 392–401.
- [3] T. Lozano-Perez, Spatial planning: A configuration space approach, in: Autonomous robot vehicles, Springer, 1990, pp. 259–271.
- [4] E. Behar, J.-M. Lien, Fast and robust 2d minkowski sum using reduced convolution, in: 2011 IEEE/RSJ International Conference on Intelligent Robots and Systems, IEEE, 2011, pp. 1573–1578.
- [5] N. Eckenstein, M. Yim, Modular robot connector area of acceptance from configuration space obstacles, in: 2017 IEEE/RSJ International Conference on Intelligent Robots and Systems (IROS), IEEE, 2017, pp. 3550–3555.
- [6] Y. Ma, D. Manocha, W. Wang, Efficient reciprocal collision avoidance between heterogeneous agents using CTMAT, arXiv preprint arXiv:1804.02512.
- [7] Y. Lee, E. Behar, J. M. Lien, Y. J. Kim, Continuous penetration depth computation for rigid models using dynamic Minkowski sums, Computer-Aided Design (2016) 14–25.
- [8] S. Ruan, K. L. Poblete, Y. Li, Q. Lin, Q. Ma, G. S. Chirikjian, Efficient exact collision detection between ellipsoids and superquadrics via closed-form Minkowski sums, in: 2019 International Conference on Robotics and Automation (ICRA), IEEE, 2019, pp. 1765–1771.
- [9] U. J. Römer, A. Fidlin, W. Seemann, The normal parameterization and its application to collision detection, Mechanism and Machine Theory 151 (2020) 103906.
- [10] E. Fogel, D. Halperin, C. Weibel, On the exact maximum complexity of Minkowski sums of polytopes, Discrete & Computational Geometry 42 (4) (2009) 654.

- [11] G. S. Chirikjian, A. B. Kyatkin, Harmonic analysis for engineers and applied scientists: updated and expanded edition, Courier Dover Publications, 2016.
- [12] Y. Yan, G. S. Chirikjian, Closed-form characterization of the Minkowski sum and difference of two ellipsoids, *Geometriae Dedicata* 177 (1) (2015) 103–128.
- [13] S. Ruan, Q. Ma, K. L. Pobleto, Y. Yan, G. S. Chirikjian, Path planning for ellipsoidal robots and general obstacles via closed-form characterization of Minkowski operations, in: WAFR: Proceedings of the Workshop on Algorithmic Foundations of Robotics, 2018.
- [14] J. Gravesen, Surfaces parametrized by the normals, *Computing* 79 (2-4) (2007) 175–183.
- [15] P. Hachenberger, Exact Minkowski sums of polyhedra and exact and efficient decomposition of polyhedra into convex pieces, *Algorithmica* 55 (2) (2009) 329–345.
- [16] J.-M. Lien, Covering Minkowski sum boundary using points with applications, *Computer Aided Geometric Design* 25 (8) (2008) 652–666.
- [17] H. Barki, F. Denis, F. Dupont, Contributing vertices-based Minkowski sum computation of convex polyhedra, *Computer-Aided Design* 41 (7) (2009) 525–538.
- [18] J.-M. Lien, Point-based Minkowski sum boundary, in: 15th Pacific Conference on Computer Graphics and Applications (PG’07), IEEE, 2007, pp. 261–270.
- [19] L. E. Kavradi, Computation of configuration-space obstacles using the fast Fourier transform, *IEEE Transactions on Robotics and Automation* 11 (3) (1995) 408–413.
- [20] J.-M. Lien, A simple method for computing Minkowski sum boundary in 3D using collision detection, in: WAFR: Proceedings of the Workshop on Algorithmic Foundations of Robotics, Springer, 2009, pp. 401–415.
- [21] A. Baram, E. Fogel, D. Halperin, M. Hemmer, S. Morr, Exact Minkowski sums of polygons with holes, *Computational Geometry* 73 (2018) 46–56.
- [22] C. L. Bajaj, M.-S. Kim, Generation of configuration space obstacles: The case of moving algebraic curves, *Algorithmica* 4 (1-4) (1989) 157–172.
- [23] I.-K. Lee, M.-S. Kim, G. Elber, Polynomial/rational approximation of Minkowski sum boundary curves, *Graphical Models and Image Processing* 60 (2) (1998) 136–165.
- [24] H. Mhlthaler, H. Pottmann, Computing the Minkowski sum of ruled surfaces, *Graphical Models* 65 (6) (2003) 369–384.

- [25] M. Peternell, T. Steiner, Minkowski sum boundary surfaces of 3D-objects, *Graphical Models* 69 (3-4) (2007) 180–190.
- [26] J. Mizrahi, S. Kim, I. Hanniel, M. S. Kim, G. Elber, Minkowski sum computation of B-spline surfaces, *Graphical Models* 91 (2017) 30–38.
- [27] E. Fogel, D. Halperin, Exact and efficient construction of Minkowski sums of convex polyhedra with applications, *Computer-Aided Design* 39 (11) (2007) 929–940.
- [28] G. S. Chirikjian, B. Shiffman, Closed-form parametric equation for the Minkowski sum of m ellipsoids in R^N and associated volume bounds, in review.
- [29] J.-M. Lien, Hybrid motion planning using Minkowski sums, *Proceedings of robotics: science and systems IV*.